# Polarization charges and electric quadrupole transitions of yrast terminating bands in $^{44,46,48}$Ti

Hai-liang Ma,[1,*] Bao-guo Dong,[1,2] Yu-liang Yan,[1] and Xi-zhen Zhang[1]

[1]*Department of Nuclear Physics, China Institute of Atomic Energy, Post Office Box 275(18), Beijing 102413, People's Republic of China*

[2]*Center of Theoretical Nuclear Physics, National Laboratory of Heavy Ion Collision, Lanzhou 730000, People's Republic of China*

(Received 18 March 2009; revised manuscript received 25 May 2009; published 21 July 2009)

The polarization charges in $^{44,46,48}$Ti are studied by the microscopic particle-vibration model and used to investigate the electric quadrupole transitions of the yrast terminating bands. The validity of the commonly used empirical effective charges in the $pf$ shell-model calculations is confirmed. The quadrupole transition probabilities $B(E2, I \to I-2)$ and electromagnetic moments are reasonably well reproduced compared with experimental results. It is found that a globally decreasing $B(E2)$ is accompanied with convergence of valence particles into the $1f_{7/2}$ shell when approaching the terminating states. The $I = 6^+$ state in $^{48}$Ti shows an exotic behavior with an irregularity of $B(E2)$ and sign change of electromagnetic moments, which is related to a neutron-dominant prolate shape.

DOI: 10.1103/PhysRevC.80.014316 PACS number(s): 21.60.Cs, 23.20.−g, 27.40.+z

## I. INTRODUCTION

In the $40 < A < 50$ mass region with valence particles occupying $pf$ orbitals, the termination of rotational bands has been a hot topic for decades. A great amount of spectroscopic information has been acquired and numerous electromagnetic transitions have been measured. As proton and neutron numbers are close to the middle of the $1f_{7/2}$ shell, these nuclei are nearly perfect rotors in which the interplay between single-particle and collective degrees of freedom are well manifested. Theoretically, microscopic and macroscopic models have been applied to this region, in which the shell model provides the most successful description (see Refs. [1,2]).

Effective charges have been commonly used in shell-model calculations to study electric quadrupole moments and transitions. Their microscopic origin has been traced back to the coupling between single-particle states and collective giant resonances (GRs). Core polarization charges have been studied with microscopic particle-vibration models [3–7], in which the Hartree-Fock (HF) method and random-phase approximation (RPA) are used to calculate the single-particle wave functions and giant resonances. Most of those studies concentrated on the doubly magic nuclei, since the pairing and shape deformation do not need to be considered. Some other attempts have also been directed at the isospin dependence of polarization charges in C isotopes and applied to the electric quadrupole moments in C and B isotopes [8,9].

The electromagnetic properties of terminating bands are of interest because they can provide information on the structures inside nuclei, such as deformation and configuration. Intensive shell model studies have been carried out on the electromagnetic transition properties of the terminating bands in the $pf$ shell nuclei, such as $^{48}$Cr [1], $^{44,46}$Ti and $^{49}$Cr [2], and $^{48,49}$V [10]. In these studies, the electromagnetic transition properties are calculated with empirical effective charges and harmonic oscillator wave functions. In this paper, we use the particle-vibration model to calculate the polarization charges in $^{44,46,48}$Ti. Then, the electric quadrupole transition probabilities $B(E2, I \to I-2)$ of the yrast terminating bands in these nuclei are calculated by two methods, one using the microscopic polarization charges with HF wave functions and the other using the empirical effective charges with harmonic oscillator wave functions. It is hoped that these efforts can help to clarify the validity of the widely used effective charges. The electromagnetic moments are also given to have a better understanding of the structures of these terminating bands in $^{44,46,48}$Ti.

## II. POLARIZATION CHARGES: MODEL AND FORMULAS

In normal shell-model calculations, the configurations are restricted in one or two adjacent major shells; thus the effective operators, $\tilde{O}$, have to be introduced to account for the restriction of the Hilbert space,

$$\langle\Psi|O|\Psi\rangle = \langle\tilde{\Psi}|\tilde{O}|\tilde{\Psi}\rangle. \quad (1)$$

The most important configurations neglected in the restricted shell-model calculations are those based on one-particle one-hole excitation (with most of them involved in giant resonances), which can be treated in the RPA calculations.

In this paper, we first perform the Skyrme-HF calculations in coordinate space, then solve the RPA Green's function using the same interaction consistently. The neutron and proton degrees of freedom are taken into account explicitly in the RPA calculations. The RPA Green's function is expressed as [11–13]

$$G_{\mathrm{RPA}} = G^{(0)} + G^{(0)} V G_{\mathrm{RPA}} = (1 - G^{(0)}V)^{-1} G^{(0)}, \quad (2)$$

where $G^{(0)}$ is the unperturbed Green's function and $V$ is the particle-hole interaction deduced from the Skyrme interaction. In the continuum RPA formulism, the RPA strength function is obtained by

$$S(E) = \sum_n |\langle n|Q|0\rangle|^2 \delta(E - E_n) = \frac{1}{\pi} \mathrm{Im\,Tr}(Q^\dagger G_{\mathrm{RPA}}(E) Q), \quad (3)$$

*mhl624@ciae.ac.cn

 

where $Q$ is the one-body operator. The isoscalar (IS) and isovector (IV) quadrupole operators are defined as follows:

$$Q_\mu^{\lambda=2,\mathrm{IS}} = \sum_{i=1}^{A} r_i^2 Y_{2\mu}(\hat{r}_i), \tag{4}$$

$$Q_\mu^{\lambda=2,\mathrm{IV}} = \sum_{i=1}^{A} \tau_z r_i^2 Y_{2\mu}(\hat{r}_i). \tag{5}$$

Here for protons $\tau_z = -1$ and for neutrons $\tau_z = 1$ and $A$ is the mass number. The electric quadrupole operator then can be written as

$$Q_\mu^{\lambda=2,\mathrm{el}} = e\sum_{i=1}^{Z}(1-\tau_z) r_i^2 Y_{2\mu}(\hat{r}_i) = \frac{e}{2}\left(Q_\mu^{\lambda=2,\mathrm{IS}} - Q_\mu^{\lambda=2,\mathrm{IV}}\right). \tag{6}$$

A particle-vibration method with RPA phonons can be used to estimate the polarization resulting from the core excitation [3–7]. The perturbed single-particle wave function is expressed as

$$|\tilde{i}\rangle = |i\rangle + \sum_{j,\omega_\lambda} \frac{\langle (j\otimes\omega_\lambda)i|V_{\mathrm{pv}}|i\rangle}{\varepsilon_i - (\varepsilon_j + \omega_\lambda)} |(j\otimes\omega_\lambda)i\rangle, \tag{7}$$

where $\varepsilon_i$ and $\omega_\lambda$ are single-particle energy and phonon excitation energy, $|(j\otimes\omega_\lambda)i\rangle$ is the coupled single-particle wave function with a quadrupole phonon, and $V_{\mathrm{pv}}$ is the particle-vibration coupling interaction [3,14], based on the same Skyrme interaction in the HF and RPA calculations.

The reduced matrix for one-body operator is modified as

$$\langle \tilde{j}\|Q_\lambda\|\tilde{i}\rangle = \langle j\|Q_\lambda\|i\rangle + \sum_{\omega_\lambda} \frac{2\omega_\lambda}{(\varepsilon_i-\varepsilon_j)^2 - \omega_\lambda^2} \times \frac{\sqrt{2i+1}\langle (j\otimes\omega_\lambda)i|V_{\mathrm{pv}}|i\rangle}{\sqrt{2\lambda+1}} \langle \omega_\lambda\|Q_\lambda\|0\rangle. \tag{8}$$

The particle-vibration coupling $V_{\mathrm{pv}}$ is derived from the Skyrme interaction by approximating the momentum derivative operators $\boldsymbol{k}$ and $\boldsymbol{k}'$ by the Fermi momentum $\boldsymbol{k}_F$ so that one can use directly the RPA transition densities for the calculation of the matrix element [3,7]. Then we have

$$V_{\mathrm{pv}}(\boldsymbol{r}_1 - \boldsymbol{r}_2) = \delta(\boldsymbol{r}_1 - \boldsymbol{r}_2)\left(V_{\mathrm{pv}}^{\mathrm{IS}}(r) + \tau_z(1)\tau_z(2)V_{\mathrm{pv}}^{\mathrm{IV}}(r)\right), \tag{9}$$

where

$$V_{\mathrm{pv}}^{\mathrm{IS}}(r) = \left\{\tfrac{3}{4}t_0 + \tfrac{3}{48}(\alpha+2)(\alpha+1)t_3\rho^\alpha(r) + \tfrac{1}{8}k_{\mathrm{F}}^2[3t_1 + t_2(5+4x_2)]\right\}, \tag{10}$$

$$V_{\mathrm{pv}}^{\mathrm{IV}}(r) = \left\{-\tfrac{1}{4}t_0(1+2x_0) - \tfrac{1}{24}t_3(1+2x_3)\rho^\alpha(r) + \tfrac{1}{8}k_{\mathrm{F}}^2[-t_1(1+2x_1) + t_2(1+2x_2)]\right\} \tag{11}$$

$$r = \tfrac{1}{2}(r_1 + r_2). \tag{12}$$

Then the coupling matrix can be evaluated to be

$$\langle (j\otimes\omega_\lambda)i|V_{\mathrm{pv}}|i\rangle = \frac{1}{\sqrt{2i+1}}\int r^2 \mathrm{d}r\, V_{\mathrm{pv}}(r)\delta\rho_\lambda R_j(r)R_i(r) \times \langle j\|Y_\lambda\|i\rangle, \tag{13}$$

where $R_j(r)$ is the radial single-particle wave function and $\delta\rho(r)$ is the normalized radial transition density defined as

$$\delta\rho(\boldsymbol{r}) \equiv \delta\rho(r)Y_{\lambda\mu}(\hat{\boldsymbol{r}}). \tag{14}$$

In the present proton-neutron formulism, both the isoscalar and isovector parts are included in the particle-vibration coupling $V_{\mathrm{pv}}$,

$$V_{\mathrm{pv}}\delta\rho(r) = V_{\mathrm{pv}}^{\mathrm{IS}}(r)[\delta\rho_n(r) + \delta\rho_p(r)] + \tau_z^{\mathrm{particle}} V_{\mathrm{pv}}^{\mathrm{IV}}(r)[\delta\rho_n(r) - \delta\rho_p(r)], \tag{15}$$

where for calculating neutron (proton) effective charges, we take $\tau_z^{\mathrm{particle}} = 1\ (-1)$.

For the electric quadrupole operator, the effective charges are given by

$$e_{\mathrm{eff}} = \frac{\langle \tilde{j}\|Q^{\lambda=2,\mathrm{el}}\|\tilde{i}\rangle}{\langle j\|Q^{\lambda=2,\mathrm{IS}}\|i\rangle}. \tag{16}$$

The polarization charges are related to the effective charges by

$$e_{\mathrm{pol}} = e_{\mathrm{eff}} - \left(\tfrac{1}{2} - t_z\right), \tag{17}$$

where $t_z$ is the third component of the isospin (for proton/neutron $t_z = -1/2$). Equivalently, by invoking Eq. (6), the polarization charges $e_{\mathrm{pol}}$ can be decomposed into IS and IV parts,

$$e_{\mathrm{pol}} = \frac{e}{2}\left(\chi_{\mathrm{pol}}^{\mathrm{IS}} - \chi_{\mathrm{pol}}^{\mathrm{IV}}\right), \tag{18}$$

where $\chi_{\mathrm{pol}}^{\mathrm{IS}}$ and $\chi_{\mathrm{pol}}^{\mathrm{IV}}$ are IS and IV polarizabilities given by

$$\chi_{\mathrm{pol}}^{\mathrm{IS}} = \frac{\langle \tilde{j}\|Q^{\lambda=2,\mathrm{IS}}\|\tilde{i}\rangle}{\langle j\|Q^{\lambda=2,\mathrm{IS}}\|i\rangle} - 1, \tag{19}$$

$$\chi_{\mathrm{pol}}^{\mathrm{IV}} = \frac{\langle \tilde{j}\|Q^{\lambda=2,\mathrm{IV}}\|\tilde{i}\rangle}{\langle j\|Q^{\lambda=2,\mathrm{IV}}\|i\rangle} - 1. \tag{20}$$

In principle, Eq. (18) and Eq. (17) should give the same results.

In the present continuum calculation, the transition densities at given energy are likely to be a superposition of contributions from many states with different dynamic structure. Thus, the neutron (proton) part of the IS transition density $\delta\rho_n^{\mathrm{IS}}$ ($\delta\rho_p^{\mathrm{IS}}$) at a given energy may not necessarily be the same as that of the IV transition density $\delta\rho_n^{\mathrm{IV}}$ ($\delta\rho_n^{\mathrm{IV}}$), in contrast to the case of an isolated quantum state. In the calculation of $e_{\mathrm{pol}}$, $\chi_{\mathrm{pol}}^{\mathrm{IS}}$, and $\chi_{\mathrm{pol}}^{\mathrm{IV}}$, the transition densities should be obtained from electric, IS, and IV external probes, respectively.

## III. POLARIZATION CHARGES IN $^{44,46,48}$Ti

The Skyrme-HF plus RPA calculations are performed for $^{44,46,48}$Ti using the SKM* interaction [15]. To obtain the HF ground state, the proton and neutron $1f_{7/2}$ orbitals are partially filled. The wave functions of continuum states ($E > 0$) are

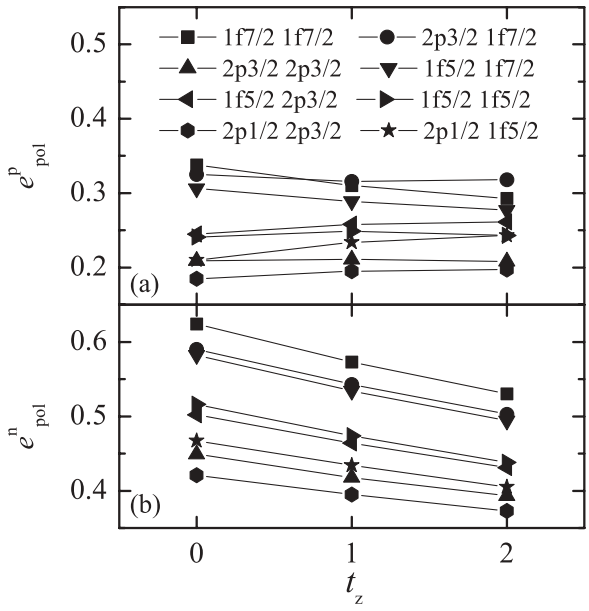


FIG. 1. Calculated state-dependent static electric quadrupole polarization effects for (a) protons and (b) neutrons in $^{44,46,48}$Ti as a function of isospin. The SKM* interaction is used. The solid lines serve as the guide for the eye.

obtained by putting the nuclei in a sphere of radius 15 fm. However, the pairing interaction and shape deformation are not included in the present study.

In the RPA calculations, the dominant peaks for the IS GR in $^{44,46,48}$Ti are found around 16.5 MeV. The IS GR exhausts 93.2%, 93.1%, and 89.4% of the classical energy-weighted sum rule [14] in $^{44,46,48}$Ti, respectively, which demonstrates that our RPA calculations are reliable.

In the calculations, considering that the excitation energy $\omega_\lambda$ is much larger than $|\varepsilon_i - \varepsilon_j|$, in the static approximation, we have $\varepsilon_i = \varepsilon_j$ in Eq. (7). The trends of static polarization effects as a function of the third component of isospin $t_z$ are shown in Fig. 1. The commonly used empirical polarization charges in the $pf$ shell are $e^n_{\rm pol} = e^p_{\rm pol} = 0.5$. In Fig. 1, the microscopic $e^p_{\rm pol}$ are less than 0.5 and $e^n_{\rm pol}$ are a bit larger than 0.5 for the $1f_{7/2}$ orbitals. The main difference between calculated and empirical polarization charges comes from proton orbitals.

The microscopic polarization charges in Fig. 1 show a quenching effect from $1f_{7/2}$ to $2p_{1/2}$ orbitals. Since the peak ($r \sim 4.0$ fm) of the transition density $\rho(r)$ at the IS GR is near the peak of the $1f_{7/2}$ radial wave function ($r \sim 3.9$ fm), their overlap will be larger than that between $\rho(r)$ and other orbitals. As we can see from Eqs. (8) and (17), this will lead to larger polarization charges in the $1f_{7/2}$ orbitals.

## IV. ELECTROMAGNETIC TRANSITIONS OF YRAST PARITY BANDS IN $^{44,46,48}$Ti

The termination values of yrast bands in $^{44,46,48}$Ti are reported in Refs. [16–19]. Relative to a $^{40}$Ca doubly magic core, in $^{44,46,48}$Ti, there are two valence protons and 2, 4, and 6 valence neutrons for the yrast ($\pi = +$) states. With all

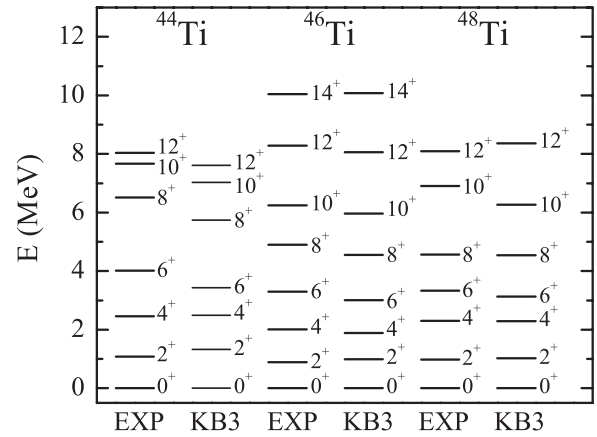


FIG. 2. Comparison of theoretical and experimental energy levels of yrast bands in $^{44,46,48}$Ti.

valence particles aligned, the yrast bands will terminate at spin $I = 12^+$, $14^+$, and $12^+$, respectively.

In our shell-model calculations, the NUSHELLX code [20] with the full $pf$ shell and KB3 [1] residual interaction is used. The experimental and calculated energy levels are shown in Fig. 2, where the energies of ground states $0^+$(g.s.) have been set to zero in three cases. We can see that the KB3 interaction has reasonably well reproduced the experimental energy levels up to the band terminations.

The electric quadrupole transition matrix elements between the final state $|J_f\rangle$ and initial state $|J_i\rangle$ involving effective operators are usually defined as

$$\begin{aligned}\langle J_f \| \tilde{Q}^{\lambda=2,\rm el} \| J_i \rangle &= A_p e^p_{\rm eff} + A_n e^n_{\rm eff} \\ &= A_p \left(1 + e^p_{\rm pol}\right) + A_n e^n_{\rm pol}, \end{aligned} \tag{21}$$

where $A_p$ and $A_n$ are proton and neutron matrix elements with bare operators using proton and neutron wave functions, respectively. The sum is implicit for the orbitals within the shell-model valence space. The electric quadrupole reduced transition probability then reads

$$B(E2, J_i \to J_f) = \frac{|\langle J_f \| \tilde{Q}^{\lambda=2,\rm el} \| J_i \rangle|^2}{2J_i + 1}. \tag{22}$$

The experimental and theoretical $B(E2, I \to I-2)$ values are shown in Fig. 3. Based on the one-body transition matrix elements given by the shell-model calculations, the quadrupole transition matrix between $I\hbar$ and $(I-2)\hbar$ states of yrast terminating bands in $^{44,46,48}$Ti is calculated by two methods. The one labeled as PV in Fig. 3 uses the microscopic polarization charges and the HF wave functions. The other labeled as HO uses empirical effective charges with harmonic oscillator wave functions. In the PV method, the HF wave functions using the SKM* interaction [15] are applied to estimate polarization effects as well as estimate reduced matrix elements when calculating $B(E2)$. In the HO method, we use the oscillator parameter $\hbar\omega \approx 45A^{-1/3} - 25A^{-2/3}$ [23], where $A$ is the mass number and the commonly used empirical effective charges are $e^p_{\rm eff} = 1.5$ and $e^n_{\rm eff} = 0.5$. In Fig. 3, some experimental $B(E2)$ values are calculated from the

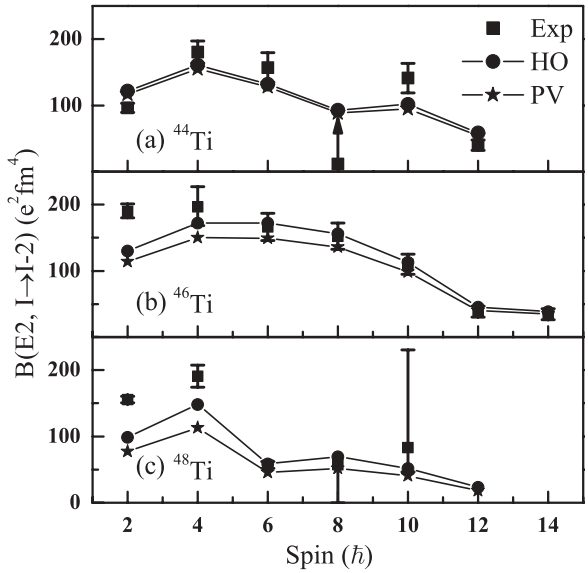


FIG. 3. Experimental and theoretical $B(E2, I \to I-2)$ of the yrast terminating bands. The solid squares, circles, and stars correspond to the experimental, PV, and HO results. The experimental values of $^{44}$Ti as well as $B(E2, 8^+ \to 6^+)$ and $B(E2, 10^+ \to 8^+)$ in $^{48}$Ti are calculated from lifetime measurements [21,22], using Eq. (23); in $^{46}$Ti, they are taken from Ref. [18]. The up arrow at $8^+$ in $^{44}$Ti means that the deduced experimental value is larger than the value of the arrow end.

half-lifetime $t_{1/2}$ by the following equation:

$$B(E2) = \ln(2) \big/ \left(1.22 \times 10^{-3} t_{1/2} E_\gamma^5\right), \tag{23}$$

with $t_{1/2}$ in picoseconds, $E_\gamma$ in MeV, and $B(E2)$ in $e^2$ fm$^4$.

We see in Fig. 3 that the calculated $B(E2)$ values have reproduced experimental results reasonably well especially in the high-spin region. The overall decreasing $B(E2)$ is related to the decreasing collectivity of these bands as they gradually approach terminating states, which is well established in mean-field studies of terminating bands.

In Table I, we present the shell-model results of the occupation percentage of the configuration with all valence particles occupying the $1f_{7/2}$ orbitals. An interesting phenomena is that the trend of $f_{7/2}^{A-40}$ configuration occupation percentage is reverse to that of $B(E2)$, which means that the gradual alignment of valence nucleons is accompanied by the convergence of valence particles into the $1f_{7/2}$ orbitals, whereas, at the terminating states, the configurations are almost pure $f_{7/2}^{A-40}$. At this time, the $A-40$ valence particles occupy the $7/2^-, 5/2^-, 3/2^-, \ldots,$ single-particle orbitals, and thus the single-particle freedom is almost fully manifested. In other words, the mixing of $t > 0$ states, where $t$ is the number of nucleons excited from $1f_{7/2}$ to upper orbitals, is less important at high spin for $1f_{7/2}$ rotors.

TABLE I. Occupation percentage of the $f_{7/2}^{A-40}$ configuration at $I^+$ for the yrast terminating bands in $^{44,46,48}$Ti, where $A-40$ is the valence particle number outside the $^{40}$Ca core.

| $I^+(\hbar)$ | 0 | 2 | 4 | 6 | 8 | 10 | 12 | 14 |
|---|---|---|---|---|---|---|---|---|
| $^{44}$Ti | 57.1 | 46.9 | 41.5 | 51.5 | 61.4 | 75.4 | 95.1 | |
| $^{46}$Ti | 53.7 | 46.4 | 45.0 | 51.6 | 54.5 | 64.3 | 83.0 | 88.8 |
| $^{48}$Ti | 58.3 | 55.4 | 56.6 | 64.4 | 69.3 | 72.3 | 84.4 | |

In Fig. 3, the irregularities at $I = 6^+$ are also reproduced very well. This kind of irregularity near $I = 6^+$ can also be seen in some other even-even $pf$ rotors, such as $^{48}$Cr [1], $^{52}$Cr [24], $^{54}$Cr [25], $^{56}$Fe [26], and $^{58}$Fe [27], which is normally related to the alignment of the valence pair. Again, the convergence in the $f_{7/2}$ orbitals can be seen from Table I, where comparing the $6^+$ with $4^+$ states we see that the occupation percentage in the $f_{7/2}$ orbitals has suddenly increased, as $B(E2, 6^+ \to 4^+)$ drops.

To understand the mechanism of the irregularities, we calculate the electromagnetic moments of the yrast states with the HO method and bare $g$ factors in $^{44,46,48}$Ti (see Table II). In $^{48}$Ti, the proton and neutron contributions to the moments are also given. The experimental values are fairly reproduced. In the low-spin region, the KB3 interaction has underestimated the moments in $^{46,48}$Ti. As we can see in Fig. 3, the values of $B(E2, 2^+ \to 0^+_{\text{g.s.}})$ in $^{46,48}$Ti have also been underestimated. We know that the magnetic moment $\mu$ serves as a good testing of nuclear configurations; thus the underestimation of $\mu$ in $^{46,48}$Ti together with the underestimation of electric quadrupole moments $Q$ demonstrates the lack of cross-shell excitations from $sd$ to $pf$ for these two isotopes. We can also see from Table II that, in general, $\mu$ increases with increasing spin owing to the increasing contribution from spin terms. However, there is an unexpected drop at $6_1^+$ in $^{48}$Ti. The sign of $\mu(6_1^+)$ becomes negative. In our shell-model calculation, the percentage of the most important configuration, where neutrons have a full contribution to the $6^+$ state and protons have no contribution, is 46.3%. The bare $g$ factors used in this paper are $g_p^l = 1.0$, $g_p^s = 5.586$ for protons and $g_n^l = 0.0$, $g_n^s = -3.826$. Thus a neutron-dominant configuration will give a small proton contribution and a negative neutron contribution to the total magnetic moment.

In Table II, accompanied with a sign change of magnetic moment, in $^{48}$Ti at $6^+$, the calculated quadrupole moment $Q$ and the proton and neutron contributions also show sign changes. This phenomena is interesting since it demonstrates that the nuclei suffers a violent change in its shape [with positive (negative) $Q$ indicating a prolate (oblate) shape]. For two-proton particles or two-neutron holes in the $1f_{7/2}$ orbitals coupling to $2\hbar$, $4\hbar$, and $6\hbar$, with the HO method, their contribution to $Q$ will be 11.6, 1.85, and $-20.3$ $e$ fm$^2$ and $-3.87$, $-0.615$, and 6.77 $e$ fm$^2$, respectively. At the terminating state, the real shell-model results are very close to these simple estimations. At $6^+$, the dominant configuration, of which two neutron holes are fully aligned, gives a positive $Q$. For another important configuration where protons contribute $2\hbar$ to the total spin, the percentage is 28%. This configuration will contribute a large positive $Q$, so the total $Q$ will be a large positive value.

With this picture, it is easy to understand the large $B(E2, 6^+ \to 4^+)$ drop in $^{48}$Ti, because a transition from a prolate shape to a oblate shape is greatly hindered. However, the need for experimental study of the electromagnetic moments for $6^+$ states is clearly seen.

TABLE II. Theoretical and experimental electromagnetic moments of the yrast states in $^{44,46,48}$Ti. The bare $g$ factors are used in the calculation of magnetic moments. The empirical effective charges $e_p = 1.5$, $e_n = 0.5$ and harmonic oscillator wave functions are used to evaluate the electric quadrupole moments. Available experimental data are taken from Ref. [28]. Dashes indicate that there are no experimental data available yet.

| Nuclides | Experiment | | Theory | | | | | | |
|---|---|---|---|---|---|---|---|---|---|
| | $2^+$ | $4^+$ | $2^+$ | $4^+$ | $6^+$ | $8^+$ | $10^+$ | $12^+$ | $14^+$ |
| Magnetic moments ($\mu_N$) | | | | | | | | | |
| $^{44}$Ti | $1.0 \pm 0.3$ | – | 1.05 | 2.10 | 3.14 | 4.34 | 5.44 | 6.55 | |
| $^{46}$Ti | $0.99 \pm 0.5$ | $2.3 \pm 0.7$ | 0.576 | 0.931 | 2.73 | 3.91 | 5.48 | 6.26 | 6.26 |
| $^{48}$Ti | $0.78 \pm 0.04$ | $2.2 \pm 0.5$ | 0.423 | 1.87 | *−0.502* | 5.16 | 5.87 | 6.93 | |
| $^{48}$Ti($p$) | | | 0.71 | 2.70 | 1.65 | 6.69 | 7.76 | 9.51 | |
| $^{48}$Ti($n$) | | | −0.448 | −0.828 | *−2.16* | −1.54 | −1.90 | −2.58 | |
| Electric quadrupole moments ($e$ fm$^2$) | | | | | | | | | |
| $^{44}$Ti | – | – | −12.9 | −23.0 | −31.6 | −23.6 | −24.8 | −29.4 | |
| $^{46}$Ti | $-21.0 \pm 6.0$ | – | −16.8 | −25.1 | −22.7 | −26.1 | −31.5 | −24.0 | −25.3 |
| $^{48}$Ti | $-17.7 \pm 0.8$ | – | −15.0 | −11.8 | *18.9* | −13.8 | −21.0 | −16.7 | |
| $^{48}$Ti($p$) | | | −8.56 | −6.60 | *12.7* | −10.4 | −18.4 | −20.7 | |
| $^{48}$Ti($n$) | | | −6.40 | −5.22 | *6.17* | −3.41 | −2.60 | 3.97 | |

## V. CONCLUSION

In summary, we have used the microscopic particle-vibration model to calculate the effective charges in $^{44,46,48}$Ti. The proton polarization charges are smaller than the empirical value of 0.5. Two methods, the theoretical effective charges with HF wave functions and the empirical charges with harmonic oscillator wave functions, are used to investigate the $B(E2, I \to I-2)$ values of the yrast terminating bands in these nuclei. Both methods have reproduced $B(E2)$ reasonably well especially near terminating states. The validity of the commonly used empirical effective charges is confirmed. We have also shown that the globally decreasing $B(E2)$ is accompanied with convergence into $1f_{7/2}$ orbitals approaching the terminating states. The $I = 6^+$ state in $^{48}$Ti has an exotic behavior with irregularity of $B(E2)$ and a sign change of electromagnetic moments. We interpret this state to be a neutron-dominant prolate state. Further experimental studies on this state are required and welcome.


[1] E. Caurier *et al.*, Rev. Mod. Phys. **77**, 427 (2005).
[2] A. Juodagalvis, I. Ragnarsson, and S. Åberg, Phys. Rev. C **73**, 044327 (2006).
[3] H. Sagawa and B. A. Brown, Nucl. Phys. **A430**, 84 (1984).
[4] I. Hamamoto and H. Sagawa, Phys. Rev. C **54**, 2369 (1996).
[5] I. Hamamoto, H. Sagawa, and X. Z. Zhang, Nucl. Phys. **A626**, 669 (1997).
[6] I. Hamamoto and H. Sagawa, Phys. Lett. **B394**, 1 (1997).
[7] C. L. Zhang, H. Q. Zhang, X. Z. Zhang, H. Sagawa, and F. R. Xu, J. Phys. G: Nucl. Part. Phys. **32**, 2261 (2006).
[8] T. Suzuki, H. Sagawa, and K. Hagino, Phys. Rev. C **68**, 014317 (2003).
[9] H. Sagawa and K. Asahi, Phys. Rev. C **63**, 064310 (2001).
[10] F. Brandolini *et al.*, Phys. Rev. C **66**, 024304 (2002).
[11] G. F. Bertsch and S. F. Tsai, Phys. Rep. **18**, 125 (1975).
[12] S. Sholomo and G. F. Bertsch, Nucl. Phys. **A243**, 507 (1975).
[13] N. Van Giai and H. Sagawa, Nucl. Phys. **A371**, 1 (1981).
[14] A. Bohr and B. R. Mottelson, *Nuclear Structure* (Benjamin, New York, 1975), Vol. II, pp. 401, 515.
[15] J. Bartel, P. Quentin, M. Brack, C. Guet, and H. B. Hakansson, Nucl. Phys. **A386**, 79 (1982).
[16] J. J. Kolata, J. W. Olness, and E. K. Warburton, Phys. Rev. C **10**, 1663 (1974).
[17] C. D. O'Leary *et al.*, Phys. Rev. C **61**, 064314 (2000).
[18] F. Brandolini, Eur. Phys. J. A **20**, 139 (2004).
[19] F. Glatz *et al.*, Z. Phys. A **293**, 57 (1979); J. F. A. G. Ruyl, J. B. M. De Haas, P. M. Endt, and L. Zybert, Nucl. Phys. **A419**, 439 (1984).
[20] NUSHELLX for Windows and Linux, W. D. M. Rae, http://knollhouse.org (unpublished).
[21] J. A. Cameron and B. Singh, Nucl. Data Sheets **88**, 299 (1999).
[22] T. W. Burrows, Nucl. Data Sheets **107**, 1747 (2006).
[23] J. Blomqvist and A. Molinari, Nucl. Phys. **A106**, 545 (1968).
[24] H. Junde, H. Su, and M. A. Chunhui, Nucl. Data Sheets **108**, 773 (2007).
[25] H. Junde and H. Su, Nucl. Data Sheets **107**, 1393 (2006).
[26] H. Junde, Nucl. Data Sheets **86**, 315 (1999).
[27] M. R. Bhat, Nucl. Data Sheets **80**, 789 (1997).
[28] N. J. Stone, At. Data Nucl. Data Tables **90**, 75 (2005).